

DOI: 10.1002/ ((please add manuscript number))

Article type: Full Paper

Nitrogen rich hierarchically organized porous carbon/sulfur composite cathode electrode for high performance Li/S battery: A mechanistic investigation by operando spectroscopic studies

Bhaghavathi Parambath Vinayan, Thomas Diemant, Xiu-Mei Lin, Musa Ali Cambaz, Ute Golla-Schindler, Ute Kaiser, R. Jürgen Behm, Maximilian Fichtner*

Dr. Bhaghavathi Parambath Vinayan, Dr. Xiu-Mei Lin, Musa Ali Cambaz, Prof. R. Jürgen Behm, Prof. Maximilian Fichtner
Helmholtz Institute Ulm for Electrochemical Energy Storage (HIU), Helmholtzstr. 11,
D-89081 Ulm, Germany
E-mail: vinayan.parambath@kit.edu

Dr. Thomas Diemant, Prof. R. Jürgen Behm
Institute of Surface Chemistry and Catalysis, Ulm University, Albert-Einstein-Allee 47, D-89081 Ulm, Germany

Dr. Ute Golla-Schindler, Prof. Ute Kaiser
Electron Microscopy Group of Materials Science, Central Facility for Electron Microscopy, Ulm University, Albert-Einstein-Allee 11, D-89081 Ulm, Germany

Dr. Bhaghavathi Parambath Vinayan, Prof. Maximilian Fichtner
Karlsruhe Institute of Technology, Institute of Nanotechnology, P.O. Box 3640, D-76021 Karlsruhe

Keywords: hierarchical porous materials, heteroatom doping, lithium-sulfur batteries, polysulfide dissolutions, in-situ Raman

The physiochemical properties of the carbon host matrix and their sulfur loadings play a major role in the electrochemical performance of lithium-sulfur batteries. We have designed a highly sulfur loaded (75 wt.%) carbon matrix (S/NGC), with hierarchically organized micro/meso pore structures containing nitrogen and oxygen functional groups, and using metal oxide nanostructured templates. The S/NGC electrodes give reversible capacities of 868 and 666 mAh g⁻¹ at C/5 current rates, with sulfur loading of 2.2 and 3.4 mg cm⁻², respectively. Based on the advantages of the hierarchically organized porous structure and heteroatom doping, S/NGC electrode shows long cycling stability (0.03% capacity decay per cycle in the first 1000 cycles) with high coulombic efficiency (> 99 %), which is an improvement by a factor of two compared with a sulfur/graphene cathode. Further, the charge/discharge mechanism of the cell was investigated in detail by in-situ Raman and ex-situ X-ray photoelectron spectroscopy. The presence of nitrogen on the carbon support is found to make the bond formation easier between sulfur and oxygen functional groups existing at the carbon support, which is supposed to play a major role along with hierarchically organized porous structure, for the prevention of sulfur/polysulfides species dissolution to the anode side.

1. Introduction

Lithium-sulfur (Li/S) batteries are considered as one of the most promising rechargeable battery technologies for future applications due to their low cost, environment-friendly and high theoretical energy density ($\sim 2500 \text{ Wh kg}^{-1}$).^[1] The high theoretical specific capacity ($\sim 1672 \text{ mA h g}^{-1}$) of the Li/S battery is the result of a cascade of reversible two electron conversion reactions between sulfur and lithium at an average voltage of 2.1 V with respect to Li/Li^+ , which goes through a series of intermediate states of liquid polysulfides and finally leads to solid lithium sulfide ($\text{S}_8 + 16\text{Li}^+ + 16\text{e}^- \leftrightarrow 8\text{Li}_2\text{S}$).^[1b] Still, the practical implementation of the Li/S battery as successor of the currently used Li-ion battery is quite challenging and needs to address several issues. The first challenge is the insulating nature of sulfur ($1 \times 10^{-15} \text{ S m}^{-1}$) and its discharge products (Li_2S) at the cathode, which leads to a low utilization of active material and necessitates the confinement of sulfur in a conductive host matrix at the expense of the energy density of the cell.^[2] The second point is the large volumetric change ($\sim 79 \%$) between sulfur and the final product Li_2S during discharge/charge. This can lead to the pulverization of cathode material and result in loss of electronic contact between particles causing a poor mechanical stability of the cathode. Third one is the drying out of cell during cycling due to electrolyte decomposition as a result of unstable passivation layer formation at Li side.^[3] Finally, the major challenge is the polysulfide shuttling effect between the electrodes, i.e., the diffusion of liquid polysulfides from the S-containing cathode to the Li anode side, where they can get reduced to insoluble $\text{Li}_2\text{S}_2/\text{Li}_2\text{S}$. This shuttling of polysulfides leads to (i) loss of active material from the cathode side, (ii) poor cycling stability, (iii) decreased coulombic efficiency, (iv) increase in the cell internal resistance, (v) corrosion of the Li anode and (vi) self-discharge of the cell upon storage.^[4] All these issues of the Li/S battery are strongly correlated with the (a) sulfur loading at the cathode side, (b)

amount of electrolyte used in the cell and (c) physiochemical properties (dielectric constant, viscosity, ionic conductivity, etc.) of the electrolyte solvents, etc.^[2, 5] High specific capacity and cycle stability of a Li/S battery is usually observed only for low sulfur loadings ($< 1.5 \text{ mg}_{\text{sulfur}} \text{ cm}^{-2}$) at the cathode.^[6] However, the sulfur electrodes with low sulfur loadings are far from the performance of current commercially available Li-ion batteries, which typically feature a volumetric energy density of $\sim 690 \text{ Wh L}^{-1}$.^[7] Hence, it is necessary to design cathode electrodes with higher sulfur loading ($\geq 3 \text{ mg}_{\text{sulfur}} \text{ cm}^{-2}$), while maintaining a good capacity and cycle stability at the same time.^[6b, 8] Latest developments in this field include the fabrication of a prototype Li/S cell by Sion Power Corporation with a volumetric energy density of about 325 Wh L^{-1} , and gravimetric energy densities of 350 Wh kg^{-1} for the initial cycles and 250 Wh kg^{-1} after 80 cycles.^[1a, 8]

A straightforward and general approach for the manufacturing of high performance Li/S battery cathode electrodes is the melt infiltration of sulfur within a conductive carbon host matrix such as meso or micro porous carbons, hollow carbon nanofibers, carbon nanotubes, or graphene layers, etc.^[9] The confinement of sulfur and further forming polysulfides (Li_2S_x , $1 \leq x \leq 8$) within the carbon matrix can be done by either physical or chemical means. For physical confinement, it is necessary to have a porous high surface area host matrix with large pore volume. Recent reports show that a carbon host matrix tailored with a mixture of small and large pores can enhance the Li/S battery performance.^[9b] In these structures, the smaller pores ($< 5 \text{ nm}$) trap the sulfur/polysulfides, while the larger pores ($5\text{-}100 \text{ nm}$) facilitate the electrolyte's transport throughout the material and support for high sulfur loading.^[10] In chemical confinement, the surface of the carbon host matrix is functionalized/doped with various electron donor or acceptor chemical species, which can entrap sulfur and polysulfides by chemisorption. Recent studies illustrate that oxygen and nitrogen functional groups at the surface of host matrixes can effectively chemisorb sulfur/polysulfides species and reduce the

polysulfide shuttling.^[11] Furthermore, it seems promising to combine the physical and chemical entrapping of sulfur and polysulfides within the same carbon host matrix to get good performance sulfur cathodes.

To investigate the charge/discharge mechanism of Li/S cells, a multitude of different characterization techniques have been previously applied (e.g., XRD, XPS, Uv-Vis, XANES etc.), the majority of them were used in an ex-situ approach.^{[12] [13]} Since the elemental sulfur and the different polysulfide species which are forming as reaction intermediates at different stages of the discharge/charge cycle are strongly Raman active, in-situ Raman analysis of the Li/S cell is very interesting for a more thorough investigation of the battery reaction mechanism.^[13a] Based on this, we have designed a highly sulfur impregnated (~ 75 wt. %) nitrogen rich carbon host matrix with a combination of micro and meso pore outlets by a novel synthetic approach. The highly sulfur loaded cathode electrodes (2.2 or $3.4 \text{ mg}_{\text{sulfur}} \text{ cm}^{-2}$) of this nanocomposite show good specific capacity and long cyclability. Furthermore, the cell operation mechanisms have been thoroughly investigated by in-situ Raman spectroscopy and ex-situ XPS.

2. Results and Discussion

2.1 Structural and Morphological Characterization

Figure 1a-d shows the scanning and transmission electron microscopic studies of nitrogen rich carbon host matrix (NGC). The overview images in (a, b) indicate the formation of one and two dimensional carbon nanostructures within the sample (see also in (c, d) the corresponding high resolution TEM images). The HRTEM image (**Figure 1d**) gives a lattice spacing of 0.34 nm. Additionally, the high resolution electron microscopic images confirm the formation of micro (≤ 2 nm) and meso (~ 3-30 nm) pores within the sample. The electron energy loss spectrum of the C-K edge in **Figure 1f** shows a near edge structure similar to

graphite. The surface area and pore distributions of as prepared NGC and few layer graphene (G) samples were determined by nitrogen adsorption/desorption measurements, the associated BET surface areas for NGC and graphene samples are $\sim 963 \text{ m}^2 \text{ g}^{-1}$ and $450 \text{ m}^2 \text{ g}^{-1}$, respectively (Figure S1: Supporting information). The total pore volume of the NGC sample is $1.23 \text{ cm}^3 \text{ g}^{-1}$ and the pore size distribution (**Figure 2a**) reveals pores in the range of 0.5-30 nm with a sharp maximum at ~ 1 nm. The micro pores (≤ 2 nm) enable the trapping of intermediate polysulfides,^[3b] while the larger pores (3-30 nm) help to improve the electrolyte transport throughout the structure and make a high loading of sulfur possible as shown in the schematic Figure 1e. TGA (**Figure 2b**) reveals sulfur loadings of 75 wt. % and 73 wt. % within the S/NGC and S/G samples, respectively. Furthermore, TGA data also illustrate a stronger binding of sulfur within the NGC host matrix as compared to pure graphene matrix, as indicated by a ~ 15 °C higher desorption temperature of sulfur in the NGC matrix. Finally, elemental mapping of S/NGC (**Figure 3**) and S/G (Figure S2: Supporting information) nanocomposites by EDX analysis illustrate the uniform distribution of sulfur, nitrogen and oxygen, within the as prepared samples.

Figure 4 and Figure S2 (Supporting information) depict the C1s, O1s and S2p high resolution XP spectra of S/NGC (Figure 4) and S/G samples (Figure S2: Supporting information). The C1s spectrum of S/NGC (**Figure 4a**) is dominated by a peak at 284.5 eV which can be attributed to the graphene (sp^2 -hybridized C). The peak at 285.2 eV is related to carbon in sp^3 -hybridized C-C, C-H or C-S bonds. Finally, the two peaks at even higher binding energy (BE) (286.6 and 289.0 eV) are due to C-O and C=O bonds in the material. The high resolution O1s spectrum of S/NGC (**Figure 4b**) shows three peaks, which can be attributed to C-O (533.3 eV), C=O (531.0 eV) and S=O (531.7 eV) species, respectively. Comparison of the detail spectra in the O1s range of S/NGC (Figure 4b) and S/G samples (Figure S2b: Supporting information) shows an increase of the peak component at 531.7 eV in the spectrum of the

S/NGC sample, which demonstrates an increasing amount of the S=O species on the surface of the N doped S/NGC sample. The N1s XP spectra (**Figure 4c**) feature three different peaks at 398.1 eV, 400.5 eV and 404.2 eV, which are ascribed to pyridinic N (26 %), pyrrolic N (63 %) and oxidized N (11 %), respectively.^[14] The total nitrogen and oxygen contents at the surface of the S/NGC sample are 5.6 at. % and 8.8 at. %, respectively. It was demonstrated before that the addition of such dopants into the carbon lattice can enhance the affinity and binding strength of polar polysulfides/Li₂S to the nonpolar carbon atoms, and can in this way positively influence the cycle stability and rate capability of a Li/S cell.^{[15] [16]} The S2p spectra of the as prepared sample are discussed together with the results for electrochemically cycled samples below.

2.2 Electrochemical Results

The electrochemical performance of the samples was investigated by cyclic voltammetry (CV) and galvanostatic discharge/charge cycling. **Figure 5a** illustrates the CV curves of the S/NGC cathode electrode covering the potential range of the lithiation/de-lithiation process. The first cathodic peak at 2.35 V is due to the reduction of sulfur to soluble long-chain liquid polysulfides (Li₂S_x, 4 < x ≤ 8) and the second peak at 2.11 V corresponds to the reduction of higher order polysulfides to short-chain polysulfides (Li₂S_x, 1 ≤ x ≤ 4). The anodic peak at 2.38 V represents the re-oxidation of short chain lithium sulfides to higher order polysulfides and S₈. The oxidation and reduction potentials of the S/NGC electrodes from the CV are in good agreement with the galvanostatic discharge/charge voltage profiles of the S/NGC cell. Compared to that, the CV of the S/G cathode electrode (Figure S4: supporting information) shows the reduction peaks at lower potentials (2.26 V and 1.9 V) and the oxidation peak at higher potential (2.5 V), i.e., the S/G cathode shows compared to the S/NGC cathode an increased polarization. **Figure 5b** shows the charge/discharge curve of the S/NGC electrode with a sulfur loading of ~2.2 mg cm⁻², cycled at a current density of 0.05C (1C = 1672 mA

$\text{g}_{\text{sulfur}}^{-1}$). The discharge capacities for the 1st and 2nd cycle were 1242 and 1190 mAh g^{-1} , i.e., the electrode retains 95.8 % of its initial capacity. The discharge capacity decreased in the following initial cycles, which may be due to a redistribution of sulfur and an irreversible dissolution of polysulfides into the electrolyte.^[17] After 10 cycles, the capacity stabilized at 1140 mAh g^{-1} , which corresponds to 91 % of the initial capacity.

The cycling rate capability at various current rates (0.05C - 2C) of the cell with the S/NGC cathode ($2.2 \text{ mg}_{\text{sulfur}} \text{ cm}^{-2}$) is given in **Figure 5c** and the corresponding charge-discharge voltage profiles are shown in **Figure 5d**. Reversible capacities of 1140, 962, 805, 681, 515 and 310 mAh g^{-1} were obtained at constant current rates of 0.05 C, 0.1 C, 0.25 C, 0.5 C, 1 C and 2 C, respectively. The charge/discharge voltage profiles maintained the same shape from low (0.05 C) to high (2 C) current rates with slight increase in over potentials in the charge/discharge voltage plateaus. When the C rate was switched back from high (2 C) to low (0.1 C), the discharge capacity also returned to 942 mAh g^{-1} , demonstrating a very good reversibility of the S/NGC electrode. As compared to S/NGC, the sulfur/graphene composite (S/G) electrode with a sulfur loading of $2.2 \text{ mg}_{\text{sulfur}} \text{ cm}^{-2}$ gave a lower discharge capacity of $\sim 715 \text{ mAh g}^{-1}$ at a current rate of 0.2 C (**Figure 6a**).

For a successful implementation of Li/S batteries in practical applications, good cycling capacity retention is an indispensable prerequisite. Figure 6a compares the cycling performances of S/NGC and S/G electrodes over 1000 cycles at a current rate of 0.2 C. The active material loading was about $\sim 2.2 \text{ mg}_{\text{sulfur}} \text{ cm}^{-2}$. For S/NGC, the capacity decreased from the initial value of 868 mAh g^{-1} to 832, 688, and finally 581 mAh g^{-1} after 100, 500, 1000 cycles, respectively. The corresponding capacity retentions are 95.6 %, 79.3% and 66.9 %. The charge-discharge curves from initial to final cycles show voltage plateaus without any fading in average voltage (**Figure 6b**). The average capacity loss per cycle for S/NGC was

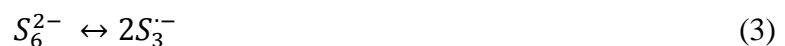
~0.033 % and the cell maintained a coulombic efficiency of 99.5 % for the whole 1000 cycles. For an S/G electrode with the same sulfur loading ($2.2 \text{ mg}_{\text{sulfur}} \text{ cm}^{-2}$), the initial capacity decreased from 715 mAh g^{-1} to 588 (100 cycles), 415 (500 cycles) and eventually 305 mAh g^{-1} (1000 cycles), i.e., 82.2 %, 58.0 % and 42.6 % of the initial capacity were maintained at these three points. When comparing to the S/NGC electrode, the S/G electrode has lower coulombic efficiency (98.4 %) and a significantly higher average capacity loss per cycle (0.057 %) at the same sulfur loading.

In the next step, the cycling performance of S/NGC electrodes with a high sulfur loading of ~ 3.4 mg cm^{-2} was tested for 350 cycles as shown in **Figure 6c**. At 0.2 C current rate, the high sulfur loaded S/NGC electrode gave an initial discharge capacity of 666 mAh g^{-1} , which decreased to 572 and 519 mAh g^{-1} after 100 and 350 cycles, respectively. This corresponds to a capacity retention of 85.9 % and 77.9 %. At this high sulfur loading of the S/NGC electrode, the average capacity loss per cycle was about 0.03 % and the cell maintained a coulombic efficiency of 99.4 % throughout the 350 cycles. For comparison, the cycle stability of an S/G electrode with the same sulfur loading was also tested again using the same current rate. The S/G electrode showed an initial discharge capacity of 558 mAh g^{-1} , which decreased to 358 mAh g^{-1} at the end of the 100th cycle (64.1 % capacity retention). The average capacity loss per cycle (0.064 %) was two times higher than that of S/NGC and the cell also had a lower coulombic efficiency of only 93.5 %.

The charge/discharge reaction mechanism or more precisely the change of the chemical state of the sulfur in the S/NGC electrode during cycling was investigated in detail by in-situ Raman spectroscopy and ex-situ XPS. **Figure 7** shows the in-situ Raman spectra and associated voltage profiles obtained for a S/NGC cathode during the discharge from 2.8 to 1.5 V (**Figure 7a-b**) followed by re-charge to 2.8 V (**Figure 7(c, d)**). The peaks in these spectra

are marked and assigned to different sulfur species according to literature.^[13a, 18] In the Raman spectrum of the as prepared S/NGC sample, the peaks at 186 cm⁻¹, 221 cm⁻¹, and 473 cm⁻¹ correspond to elemental sulfur (S₈) and the peak at 442 cm⁻¹ represents thiosulfate (S₂O₃²⁻) species originating from the surface oxy-groups.^[18b, 18c] The Raman spectrum of the pure electrolyte shows peaks at 276 and 741 cm⁻¹ (Figure S5: supporting information).

The peaks corresponding to S₈ disappear during the discharge process at 2.28V and reform upon charging at 2.30V, as shown in Figure 7. The Raman spectra suggest that the S₈ ring is reversibly decomposed and reformed during the cycling of the Li/S cell. Right at the beginning of the discharge (voltage ~2.32 V), a new peak at 533 cm⁻¹ appears which indicates the existence of an intermediate S₃^{•-} radical anion (see also below).^[19] Furthermore, another peak at 748 cm⁻¹ is detected, which is assigned to higher order polysulfide species (S_x²⁻, x=4-8). Both features gradually grow in intensity with progressing discharge (decreasing cell voltage) as shown in Figure 7a-b.^[18a] The peak at 235 cm⁻¹, which forms at ~2.28V, is assigned to S₄²⁻ species.^[18a] These new peaks are a clear indication for the stepwise conversion of S₈ to different liquid polysulfides (Li₂S_x, x=8-4) and their coexistence at the beginning of the discharge cycle (2.32 - 2.26 V). The spectra illustrate the formation of an intense S₃^{•-} peak at high discharge potentials, which could be the result of the following reactions 1, 2, and 3:



The presence of S₃^{•-} intermediate species in various ion-solvating environments was already observed in some earlier in-situ/ex-situ Li/S spectroscopic studies.^[18a] The S₆²⁻/S₃^{•-} species

can consequently be reduced to S_4^{2-}/S^{2-} .^[1b, 20] In the discharge spectra, all peaks representing the liquid polysulfides start to disappear at 2.09 V and a new broad peak at 375 cm^{-1} (corresponding to S^{2-}) starts to grow. This shows the reduction of liquid polysulfides to lower order polysulfides and the onset of the formation of the final reduction product Li_2S even at this relatively high discharge potential. At the end of the discharge cycle (1.5V), the peak corresponding to Li_2S (375 cm^{-1}) is very predominant. The presence of Li_2S was not clearly observed in earlier in-situ Raman experiments.^[18a] At this point (1.5V), peaks with small intensity corresponding to $S_3^{\bullet-}$ and S_x^{2-} ($x=4-8$) indicate the persistence of a small amount of liquid type polysulfides along with the final reduction product ‘ Li_2S ’.

During the charge, (Figure 7c-d), the intensity of the peak corresponding to Li_2S (375 cm^{-1}) starts to decrease, which evidences the re-oxidation of Li_2S . The peaks of $S_3^{\bullet-}$ (533 cm^{-1}) and S_4^{2-} (235 cm^{-1}) species show up again at 2.23 V and keep growing upon further charging until 2.28 V. After that their intensity decreases again. Additionally, the S_x^{2-} ($x = 4-8$) vibrational mode (748 cm^{-1}) shows an intense peak at 2.30 V. Beyond this point, all peaks corresponding to the liquid polysulfides loose intensity upon further charging. Instead, the S_8 peak keeps growing until the polysulfides are completely converted into S_8 by the end of the recharging (at 2.8 eV).

Recently, Nazar *et al.* reported that the thiosulfate groups ($S_2O_3^{2-}$) initially formed on the surface of the oxygen functional group containing host matrixes react with longer-chain polysulfides (Li_2S_x , $x \geq 4$) at higher discharge potential ($\geq 2.15\text{ V}$) to polythionate complexes ($S_xO_6^{2-}$, $x=3-5$) bound to the surface, along with the formation of shorter-chain polysulfides.^[21] The polythionates and shorter-chain polysulfides formed in this reaction are less soluble in the electrolyte than the longer-chain ones, leading to the retention of sulfur at

the cathode electrode.^[21] The thiosulfate formation over the surface of pristine S/NGC sample is confirmed by Raman (peak at 442 cm^{-1}) and XPS results (following section). The peak at $\sim 1065\text{ cm}^{-1}$ in the in-situ Raman spectra of the samples discharged/charged to a voltage in the range between 2.32 - 2.09 V indicates the formation of intermediate polythionate complexes ($\text{S}_x\text{O}_6^{2-}$, $x \geq 3$). At lower discharge potential, this peak disappears again (Figure 7).

The results of XPS measurements from the surface of samples at various stages of the discharge process confirm the conclusions drawn from Raman spectroscopy and give further insight into the formation of S species during discharge. For this purpose, the S2p spectra of as-prepared S/NGC and of S/NGC samples after discharge to 2.28 and 2.09 eV are presented in Figure 4d-f. The spectrum of the fresh sample is dominated by two peak doublets at 163.8/165.0 and 168.4/169.6 eV, which are assigned to elemental S and sulfate species, respectively. Furthermore, two peak couples with much lower intensity are detected at 162.2/163.4 and 167.5/168.7 eV. These are attributed to the S atoms in thiosulfate, which was also seen in the Raman spectra (peak at $\sim 442\text{ cm}^{-1}$).^[18c] In agreement to previous reports,^[21-22] the S atoms in thiosulfate show two separated peak couples due to their different surrounding: the peak doublet at higher BE (167.5/168.7 eV) is attributed to the central S atom (with O coordination), the other at lower BE (162.2/163.4 eV) is due to the peripheral S atom. It is interesting to note that the S2p spectrum of the as-prepared S/G sample (Figure S3: supporting information) shows much less thiosulfate formation, although the number of surface oxy-groups of the graphene is comparatively higher (~ 10.1 at. % O for as-prepared S/G). This indicates that the incorporation of nitrogen to an oxygen functionalized carbon host matrix can enhance the formation of thiosulfate species, which is in accordance with earlier XANES results on nitrogen doped carbon.^[11b]

After discharging to 2.28 V and 2.09 V, the reduction of sulfur manifests in the S2p XP spectra by the formation of peak doublets at lower BE, below that of the elemental S. The first doublet (162.2/163.4 eV) is assigned to the terminal S atom in polysulfides (S_x^{2-} ; $2 \leq x \leq 8$), the other one at even lower BE (160.7/161.9 eV) to the final product S^{2-} . S atoms in the middle of longer polysulfide chains (S_x^{2-} ; $x \geq 3$) should appear at a BE comparable to that of elemental S_8 and contribute to this peak couple.^[21] In agreement with expectations, the intensity of the end product (S^{2-}) increases during the discharge process. According to the literature,^[21-22] the terminal S atoms of the polythionates ($S_xO_6^{2-}$), which we identified in the Raman spectra (peak at $\sim 1065\text{ cm}^{-1}$), give rise to a S2p peak couple at 168.5/169.7 eV, i.e., approximately at the same position like SO_4^{2-} . Here, the inner S atoms contribute to the peak doublet of elemental S. Finally, another peak couple at 166.8/168.0 eV can be detected, which we assign to polythionite species ($S_yO_4^{2-}$, $y \geq 2$).^[22] It is interesting to note that the peaks due to O-coordinated S grow substantially at first when going from the as-prepared S/NGC to the sample after discharging to 2.28 V but decrease again upon further discharge (to 2.09 V). This result corroborates the findings of Raman spectroscopy that oxidized S complexes are formed in the initial stages of discharge (at high discharge voltages), which disappear again at lower potential. Furthermore, in order to unequivocally prove adsorption of higher order polysulfides (Li_2S_x , $6 \leq x \leq 8$) by the N, O functionalized carbon matrix (NGC) and their subsequent interactions, the NGC matrix was kept in Li_2S_8 polysulfide solution for 2 days, which resulted in a color change of the solution from dark red to light yellow color. This confirms the high polysulfide adsorption capability of the NGC matrix, and the subsequent reactive interaction between them, which leads to predominant appearance of low order polysulfides.^[13c, 23]

To determine the internal resistance of the cell with cycling, ac impedance measurements were carried out at different cycles (1st, 10th, 50th cycles) after charge to 2.8 V. Figure 6 shows

the Nyquist plots of the cells for S/NGC and S/G electrodes ($2.2 \text{ mg}_{\text{Sulfur}} \text{ cm}^{-2}$). The cell resistance (R_c) is the sum of solution (electrolyte + polysulfide) resistance and charge-transfer resistance of the electrodes.^[24] The values of the cell resistance for the cell with the S/NGC cathode were 24, 23 and 26 Ω after the 1st, 10th and 50th cycle, respectively. For the S/G cathode, the cell resistance values were 43, 34 and 47 Ω after the 1st, 10th and 50th cycle, respectively. The low cell resistance of the S/NGC electrode as compared to the S/G electrodes indicates a higher electrical conductivity and lower charge-transfer resistance of the S/NGC electrode as a result of its special porous morphology, N doping and stable electrode structure. It can be noticed here that the cell resistances decrease at first after the initial activation cycle but increase again after prolonged cycling, especially for the S/G electrode. This may be due to higher polysulfide dissolution and the instability of the electrode structure.

The corrosion of the Li anode electrodes during long battery cycling due to polysulfide shuttling was investigated by post mortem analysis using XPS and EDX. The sulfur content at the Li anode was quantified by XPS and EDX measurements after running the cells for 1000 cycles (0.2 C rate). Already visual inspection of the spectra (Figure S6: Supporting information) reveals for both methods a substantially larger S signal for the cell with the S/G cathode. Accordingly, the quantification of the EDX results shows S contents of 7.5 at. % (S/G) versus 3.3 at. % (S/NGC) and XPS arrives approximately at the same ratio. All of these results support the beneficial effect of carbon host matrix with a combination of hierarchically organized pore structures and the presence of nitrogen and oxygen functional groups, which can give a better trapping of liquid polysulfides and hence lower sulfur dissolution to the anode side. In addition, this material features a fast electronic/ionic transport and efficient buffering of volume changes between S_8 and Li_2S during charge/discharge cycling. These properties in combination effectively improve the current rate capability and cycling stability of the cell.

3. Conclusion

In summary, we have developed a highly sulfur loaded (75 wt. %) carbon matrix (S/NGC) material with hierarchically organized micro/meso-pore structures, which contains nitrogen and oxygen functional groups. The S/NGC cathode electrodes with sulfur loadings of 2.2 and 3.4 $\text{mg}_{\text{sulfur}} \text{cm}^{-2}$ give high specific capacities, reduced polarization and stabilized cycling performance (0.03% capacity decay per cycle up to 1000 cycles) as compared to sulfur/graphene composite. In-situ Raman spectroscopy analysis of the Li/S cell shows the formation of short chain polysulfides (S_3^- , Li_2S_x , $x = 4-1$) already at higher discharge potentials ($> 2 \text{ V}$). The incorporation of nitrogen into the carbon matrix was found to enhance the formation of bonds between sulfur and oxygen functional groups present on the carbon support (especially *via* thiosulfate formation), which is supposed to play a main role in the sulfur/polysulfides species immobilization along with hierarchical porous structure as supported by in-situ Raman and ex-situ XPS.

4. Experimental Section

Synthesis of Materials: Few layer graphene (G) was synthesized by thermal reduction and exfoliation of graphite oxide at 600 °C under argon gas atmosphere. MnO_2 nanorods were prepared by hydrothermal synthesis.^[25] Details of the synthesis of the nitrogen rich carbon host matrix (NGC) were explained in one of our previous reports.^[26] In brief, the pristine graphene was functionalized by the cationic polyelectrolyte poly(diallyl dimethyl ammonium chloride) (PDDA, 20 wt.% in H_2O) to attach positively charged surface functional groups. Pristine MnO_2 nanorods were surface functionalized with the anionic polyelectrolyte poly(sodium 4-styrenesulfonate) (PSS, M_w 70 000, 30 wt.% in H_2O). After surface functionalization, graphene and MnO_2 nanotubes were mixed together in a weight ratio of 1:1 by ultra-sonication and stirring in aqueous medium. Subsequently, the hybrid structure was

coated with the nitrogen containing polymer polypyrrole (PPy), using the monomer pyrrole (250 mL). During this process, the MnO₂ nanorods themselves act as oxidants and self-degradable templates for the formation of the porous conductive host matrix.^[26] The PPy coated hybrid structure was finally pyrolyzed at 800 °C in argon atmosphere to form a nitrogen doped porous carbon (NGC). The sulfur was loaded within NGC (S/NGC) and graphene (S/G) host matrices by melt infiltration at 155 °C and further heating at 250 °C under argon gas atmosphere.

Characterizations: The X-ray diffraction (XRD) measurements were conducted in a Stadi P diffractometer (STOE & Cie) with a MYTHEN detector using a Cu K_α X-ray source. Thermo gravimetric analysis (TGA) of the samples was carried out along with differential scanning calorimetry (DSC) using a Setaram thermal analyzer SENSYS evo instrument. The measurements were conducted from room temperature to 450 °C under helium flow (20 ml/min) with a heating rate of 10 °C min⁻¹. Brunauer-Emmett-Teller (BET) surface area analyses of the samples were performed with a Micromeritics ASAP 2020 MP system. The morphology of the samples was studied using scanning electron microscopy (SEM, LEO GEMINI 1550 VP) and transmission electron microscopy (TEM). TEM characterization of the nanocomposite was carried out using an aberration corrected FEI-TITAN 80-300 equipped with a GIF Quantum 965 energy filter and operated at 80 kV to avoid knock-on damage and increase the energy resolution.

The chemical state of the sample surfaces was determined by XPS measurements using monochromatized Al K_α (1486.6 eV) radiation (PHI 5800 MultiTechnique ESCA System, Physical Electronics). The measurements were done with a detection angle of 45°, using pass energies at the analyzer of 93.9 and 29.35 eV for survey and detail spectra, respectively. To avoid surface contamination, the samples were transferred in inert gas atmosphere to the

sample load lock of the XPS system. Samples were neutralized with electrons from a flood gun (current 3 μA) to compensate for charging effects at the surface. For binding energy calibration the C1s peak of the graphene was set to 284.5 eV. Peak fitting was done with CasaXPS using Shirley-type backgrounds and Gaussian-Lorentzian peak profiles. For the S2p peaks, doublets with peak area ratio 2:1 and spin-orbit splitting 1.2 eV were used.

Electrochemical Experiments: The electrochemical properties of the electrodes were tested using Swagelok-type cells. The electrode slurry was prepared by mixing S/NGC powder (85 wt. %) with conductive carbon (5 wt. %, Super C65) and PVDF binder (10 wt. %, Kynar) by magnetic stirring using NMP as solvent. The obtained slurry was cast onto carbon-coated aluminum foil by doctor blade techniques and thereafter dried at 60 °C for 24 h. The electrodes were prepared with two different sulfur loadings, 2.2 and 3.4 mg cm^{-2} , respectively. All cells were assembled inside an argon filled glove box with recirculation system (MBraun GmbH) and consisted of sulfur cathode, lithium anode, and polypropylene separator (Celgard 2400). The electrolyte was 1 M lithium bis(trifluoromethanesulfonyl) imide (LiTFSI, Sigma-Aldrich) dissolved in a mixture of 1,3-dioxolane (DOL, Alfa Aesar), dimethoxyethane (DME, Sigma-Aldrich) and ionic liquid (N-methyl N-butyl pyrrolidinium bis(trifluoromethanesulfonyl)imide (Pyr14TFSI), at the volume ratio 1:1:2 with 0.2 M LiNO_3 (Merck) as additive.^[27] A 20:1 electrolyte (μL) to sulfur (mg) ratio was used in each assembled cell.

Cyclic voltammetry (CV) experiments for the cells were carried out from 1.5 to 3 V at a scan rate of 0.1 mV s^{-1} using a Bio-Logic VMP-3 potentiostat. The electrochemical performance was measured galvanostatically at various C rates ($1\text{C} = 1672 \text{ mA g}_{\text{sulfur}}^{-1}$) in a voltage range of 1.7-2.8 V using an Arbin BT-2000 battery tester at room temperature. The cycling performances of all cells were tested after initial activation at C/50 current rate.^[17] The

charge/discharge specific capacities mentioned in this paper were calculated based on the mass of sulfur by excluding carbon content. Electrochemical impedance spectroscopy (EIS) was performed using an electrochemical workstation (Bio-Logic) with an applied sinusoidal excitation voltage of 5 mV in the frequency range from 100 kHz to 0.01 Hz.

In-situ Raman measurements of the Li/S cells were carried out using an ECC-Opto-Std [EL-CELL[®] GmbH] electrochemical cell connected with a confocal Raman microscope (InVia, RENISHAW). The sulfur loading at the cathode was about $\sim 3 \text{ mg cm}^{-2}$. The cathode side of the cell was sealed with a thin optical glass window (0.15 mm) and made air-tight with a rubber seal. The battery tester was an IM6 (ZAHNER-Elektrik GmbH) electrochemical workstation with “battery cycle” software. The in-situ Raman cell (EL-CELL, GmbH) was cycled between 1.5 and 2.8 V, with a constant current rate (C/20). In situ Raman spectra were collected at room temperature (ca. 22 °C) in the spectral range 100 – 1200 cm^{-1} using a HeNe laser with a wavelength of 632.8 nm as the excitation source. A 50 × objective (Carl Zeiss) was used to focus the laser light onto the electrode surface and to collect the Raman signal. Measurements were made in a backscattering configuration through the thin glass window onto the upper cathode electrode that is visible through the hole in the current collector. The laser power was $\sim 1.0 \text{ mW}$. The spectrum acquisition time was 20 s.

Supporting Information

Supporting Information is available from the Wiley Online Library or from the author.

Acknowledgements

Financial support by the Alexander *von* Humboldt Foundation, and the BMBF project “Mag-S” (grant #03XP0032E) is gratefully acknowledged. The authors would like to acknowledge Dr. Z. Zhao-Karger.

Received: ((will be filled in by the editorial staff))

Revised: ((will be filled in by the editorial staff))

Published online: ((will be filled in by the editorial staff))

References

- [1] a) Y. V. Mikhaylik, I. Kovalev, R. Schock, K. Kumaresan, J. Xu, J. Affinito, *ECS Trans.* 2010, 25, 23; b) L. F. Nazar, M. Cuisinier, Q. Pang, *MRS Bulletin* 2014, 39, 436; c) P. G. Bruce, S. A. Freunberger, L. J. Hardwick, J.-M. Tarascon, *Nat. Mater.* 2012, 11, 19.
- [2] N. Ding, S. W. Chien, T. S. A. Hor, Z. Liu, Y. Zong, *J. Power Sources* 2014, 269, 111.
- [3] a) K. Xu, *Chem. Rev. (Washington, DC, U. S.)* 2004, 104, 4303; b) L. Borchardt, M. Oschatz, S. Kaskel, *Chem. Eur. J.* 2016, 22, 1 – 29
- [4] M. Barghamadi, A. Kapoor, C. Wen, *J. Electrochem. Soc.* 2013, 160, A1256.
- [5] a) R. Xu, J. C. M. Li, J. Lu, K. Amine, I. Belharouak, *Journal of Materials Chemistry A* 2015, 3, 4170; b) S. Zhang, K. Ueno, K. Dokko, M. Watanabe, *Advanced Energy Materials* 2015, 5, 1500117.
- [6] a) M. Hagen, S. Dörfler, P. Fanz, T. Berger, R. Speck, J. Tübke, H. Althues, M. J. Hoffmann, C. Scherr, S. Kaskel, *J. Power Sources* 2013, 224, 260; b) J. Gao, H. D. Abruña, *The Journal of Physical Chemistry Letters* 2014, 5, 882.
- [7] K. M. Abraham, *The Journal of Physical Chemistry Letters* 2015, 6, 830.
- [8] M. Hagen, D. Hanselmann, K. Ahlbrecht, R. Maça, D. Gerber, J. Tübke, *Advanced Energy Materials* 2015, 5, 1401986.
- [9] a) A. Manthiram, Y. Fu, S.-H. Chung, C. Zu, Y.-S. Su, *Chem. Rev. (Washington, DC, U. S.)* 2014, 114, 11751; b) D.-W. Wang, Q. Zeng, G. Zhou, L. Yin, F. Li, H.-M. Cheng, I. R. Gentle, G. Q. M. Lu, *Journal of Materials Chemistry A* 2013, 1, 9382.
- [10] X. Ji, L. F. Nazar, *J. Mater. Chem.* 2010, 20, 9821.

- [11] a) K. Han, J. Shen, S. Hao, H. Ye, C. Wolverton, M. C. Kung, H. H. Kung, *ChemSusChem* 2014, 7, 2545; b) P. Zhu, J. Song, D. Lv, D. Wang, C. Jaye, D. A. Fischer, T. Wu, Y. Chen, *The Journal of Physical Chemistry C* 2014, 118, 7765; c) Y. Qiu, W. Li, W. Zhao, G. Li, Y. Hou, M. Liu, L. Zhou, F. Ye, H. Li, Z. Wei, S. Yang, W. Duan, Y. Ye, J. Guo, Y. Zhang, *Nano Lett.* 2014, 14, 4821; d) B. P. Vinayan, Z. Zhao-Karger, T. Diemant, V. S. K. Chakravadhanula, N. I. Schwarzburger, M. A. Cambaz, R. J. Behm, C. Kubel, M. Fichtner, *Nanoscale* 2016, 8, 3296.
- [12] R. Xu, J. Lu, K. Amine, *Advanced Energy Materials* 2015, 5, 1500408.
- [13] a) J.-T. Yeon, J.-Y. Jang, J.-G. Han, J. Cho, K. T. Lee, N.-S. Choi, *J. Electrochem. Soc.* 2012, 159, A1308; b) M. U. M. Patel, I. Arçon, G. Aquilanti, L. Stievano, G. Mali, R. Dominko, *ChemPhysChem* 2014, 15, 894; c) M. U. M. Patel, R. Dominko, *ChemSusChem* 2014, 7, 2167.
- [14] B. P. Vinayan, R. Nagar, N. Rajalakshmi, S. Ramaprabhu, *Adv. Funct. Mater.* 2012, 22, 3519.
- [15] G. Zhou, E. Paek, G. S. Hwang, A. Manthiram, *Nat Commun* 2015, 6.
- [16] a) J. Song, T. Xu, M. L. Gordin, P. Zhu, D. Lv, Y.-B. Jiang, Y. Chen, Y. Duan, D. Wang, *Adv. Funct. Mater.* 2014, 24, 1243; b) L. Ji, M. Rao, H. Zheng, L. Zhang, Y. Li, W. Duan, J. Guo, E. J. Cairns, Y. Zhang, *J. Am. Chem. Soc.* 2011, 133, 18522.
- [17] K. R. Kim, S.-H. Yu, Y.-E. Sung, *Chem. Commun. (Cambridge, U. K.)* 2016, 52, 1198.
- [18] a) H.-L. Wu, L. A. Huff, A. A. Gewirth, *ACS Appl. Mater. Interfaces* 2015, 7, 1709; b) M. Hagen, P. Schiffels, M. Hammer, S. Dörfler, J. Tübke, M. J. Hoffmann, H. Althues, S. Kaskel, *J. Electrochem. Soc.* 2013, 160, A1205; c) J. Mirza, S. R. Smith, J. Y. Baron, Y. Choi, J. Lipkowski, *Surf. Sci.* 2015, 631, 196.
- [19] Y.-C. Lu, Q. He, H. A. Gasteiger, *The Journal of Physical Chemistry C* 2014, 118, 5733.

- [20] Y. Gorlin, A. Siebel, M. Piana, T. Huthwelker, H. Jha, G. Monsch, F. Kraus, H. A. Gasteiger, M. Tromp, *J. Electrochem. Soc.* 2015, 162, A1146.
- [21] X. Liang, C. Hart, Q. Pang, A. Garsuch, T. Weiss, L. F. Nazar, *Nat Commun* 2015, 6.
- [22] K. M. Abraham, S. M. Chaudhri, *J. Electrochem. Soc.* 1986, 133, 1307.
- [23] M. U. M. Patel, R. Demir-Cakan, M. Morcrette, J.-M. Tarascon, M. Gaberscek, R. Dominko, *ChemSusChem* 2013, 6, 1177.
- [24] a) V. S. Kolosnitsyn, E. V. Kuzmina, E. V. Karaseva, S. E. Mochalov, *J. Power Sources* 2011, 196, 1478; b) Z. Deng, Z. Zhang, Y. Lai, J. Liu, J. Li, Y. Liu, *J. Electrochem. Soc.* 2013, 160, A553.
- [25] S. Lim, J. Cho, *Electrochem. Commun.* 2008, 10, 1478.
- [26] B. P. Vinayan, N. I. Schwarzburger, M. Fichtner, *Journal of Materials Chemistry A* 2015, 3, 6810.
- [27] M.-K. Song, Y. Zhang, E. J. Cairns, *Nano Lett.* 2013, 13, 5891.

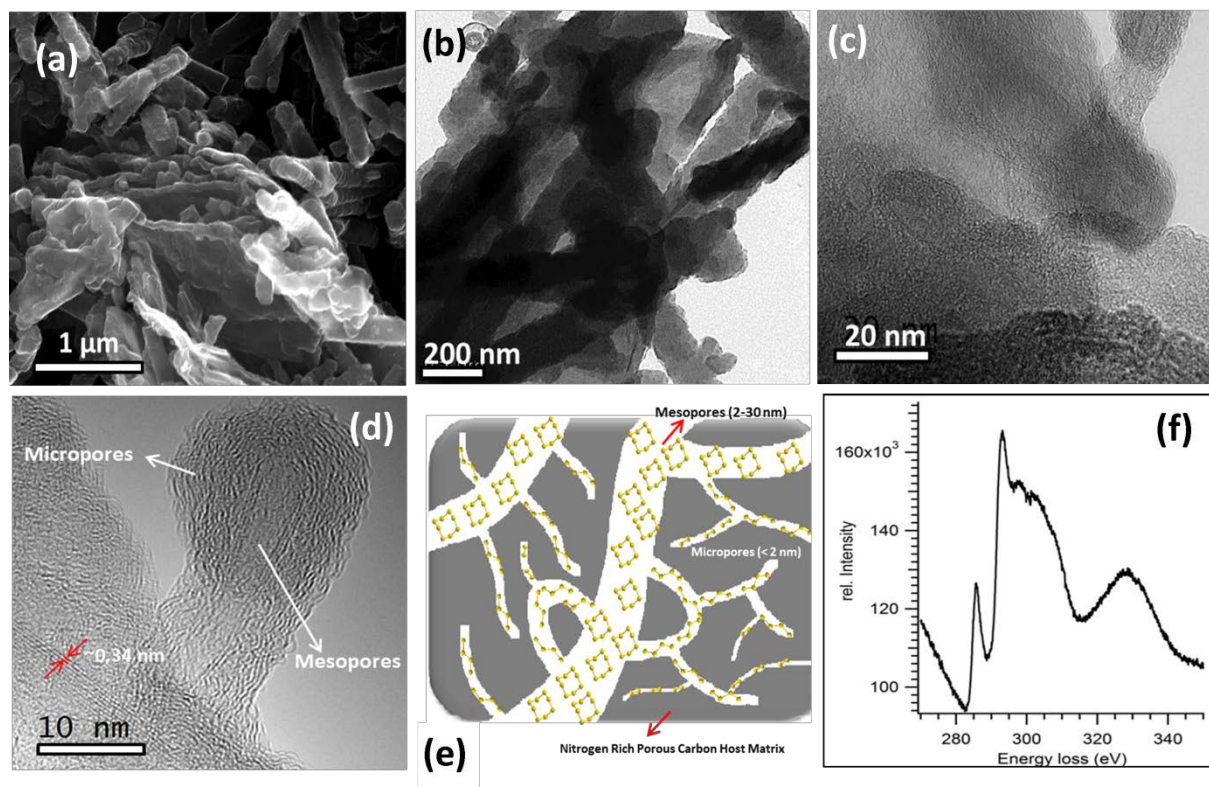


Figure 1. (a) SEM and (b) bright-field-TEM overview of NGC. (c-d) high-resolution-TEM images of NGC sample. (e) Schematic of the possible sulfur storage in the pores NGC host matrix. (f) Energy loss spectrum of the C-K edge of NGC.

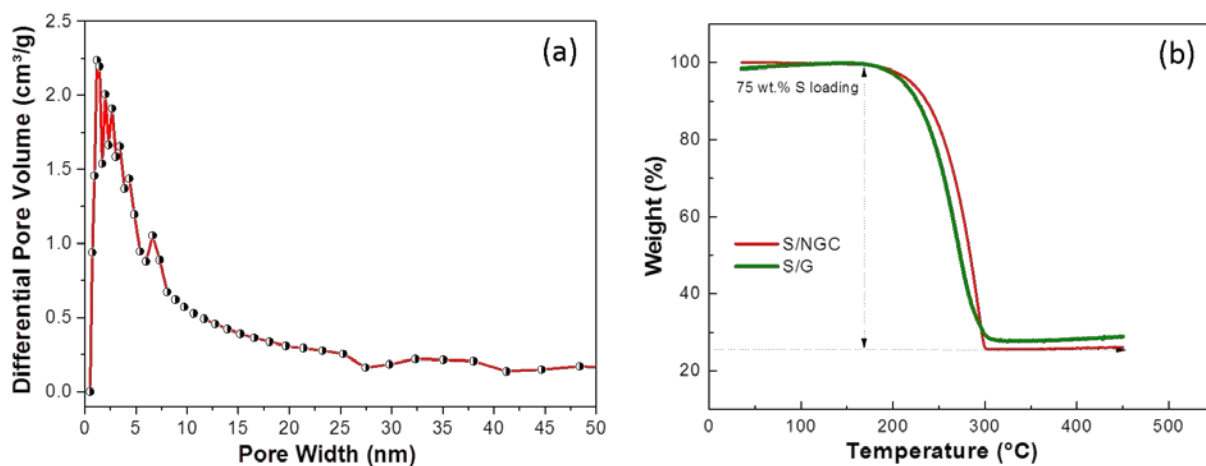


Figure 2. (a) Distribution of differential pore volume vs. pore width in NGC matrix, (b) TGA of S/NGC and S/G nanocomposite under 20 ml/min helium flow and 10 °C/min heating rate.

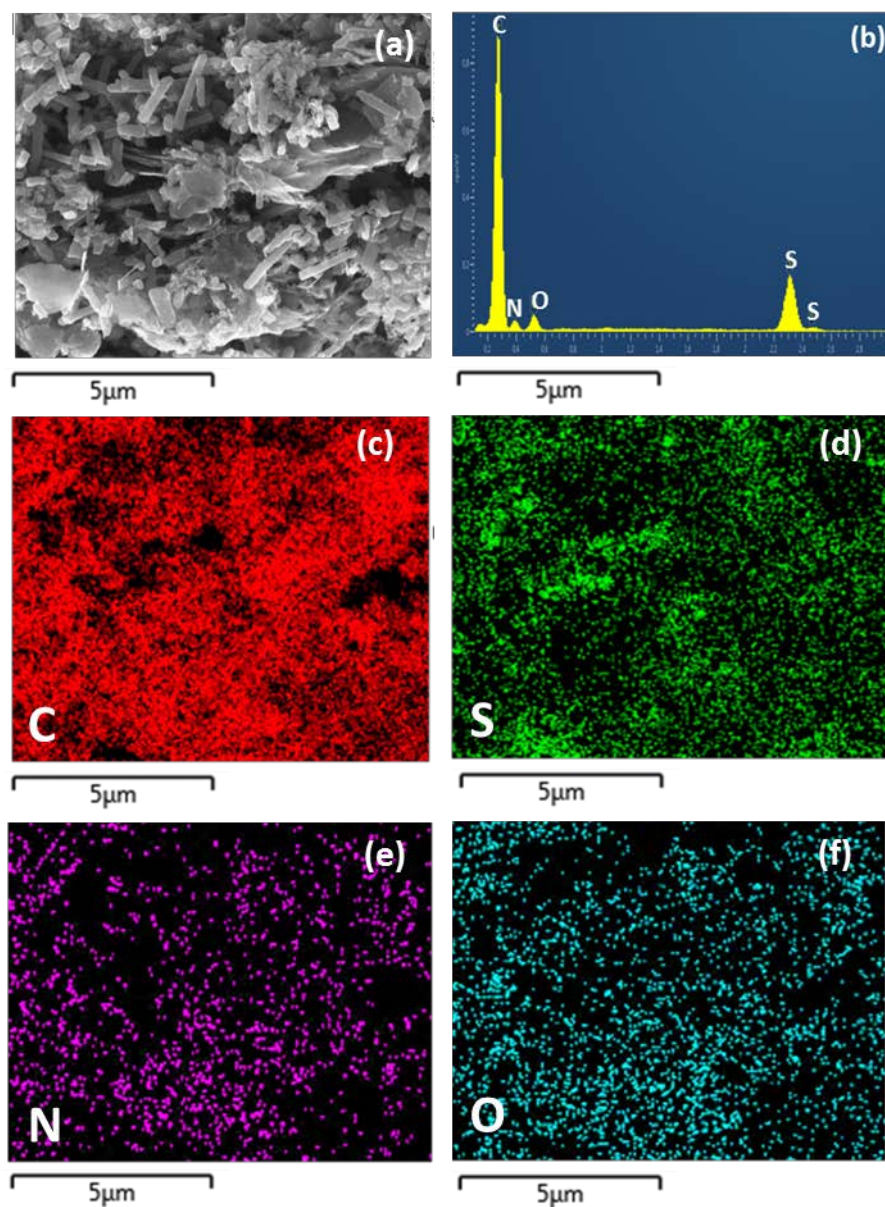


Figure 3. (a) SEM and (b) EDX of S/NGC, (c-f) elemental mapping of S/NGC nanocomposite illustrating the uniform distribution of carbon, sulfur, nitrogen and oxygen.

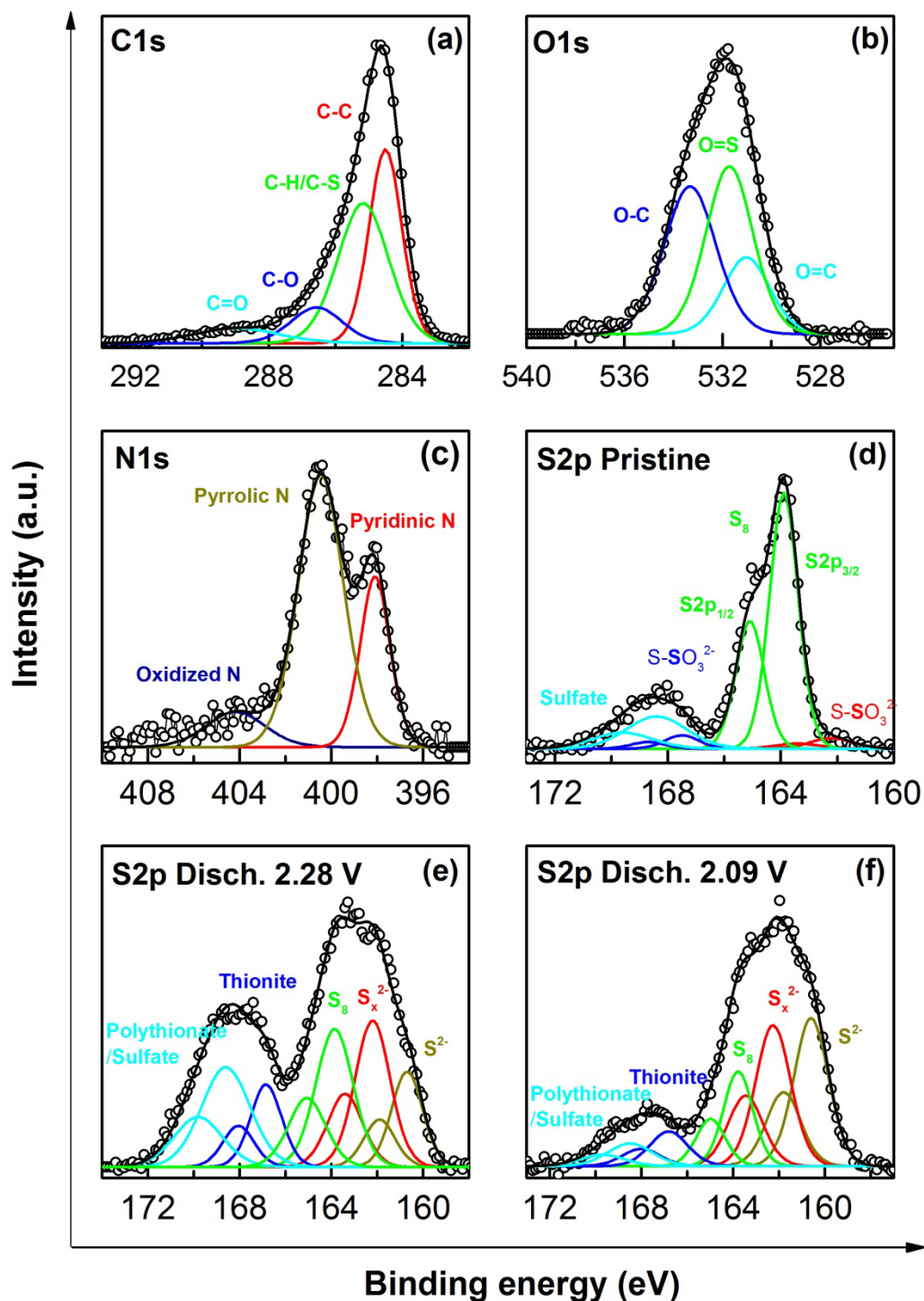


Figure 4. High resolution (a) C1s, (b) O1s, (c) N1s, and (d) S2p XP spectra of the as prepared S/NGC nanocomposite. (e-f) High resolution S2p XP spectra of an S/NGC nanocomposite electrode discharged to 2.28 V and 2.09 V.

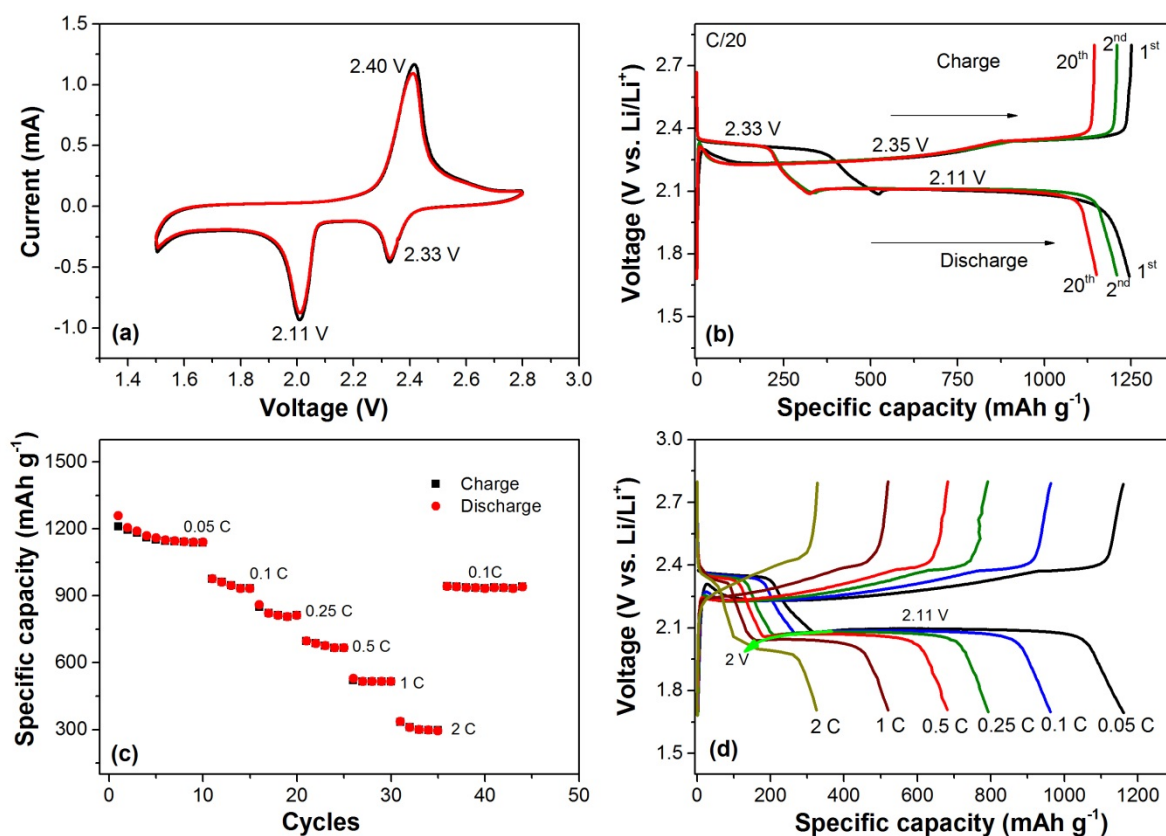


Figure 5. Electrochemical performance of S/NGC cathode electrode. (a) CV curve at 0.1 mV s⁻¹ scanning rate; (b) galvanostatic discharge/charge voltage profiles at 0.05C rate; (c) Cycle rate capability measurements, and (d) galvanostatic discharge/charge voltage profiles at various current rates.

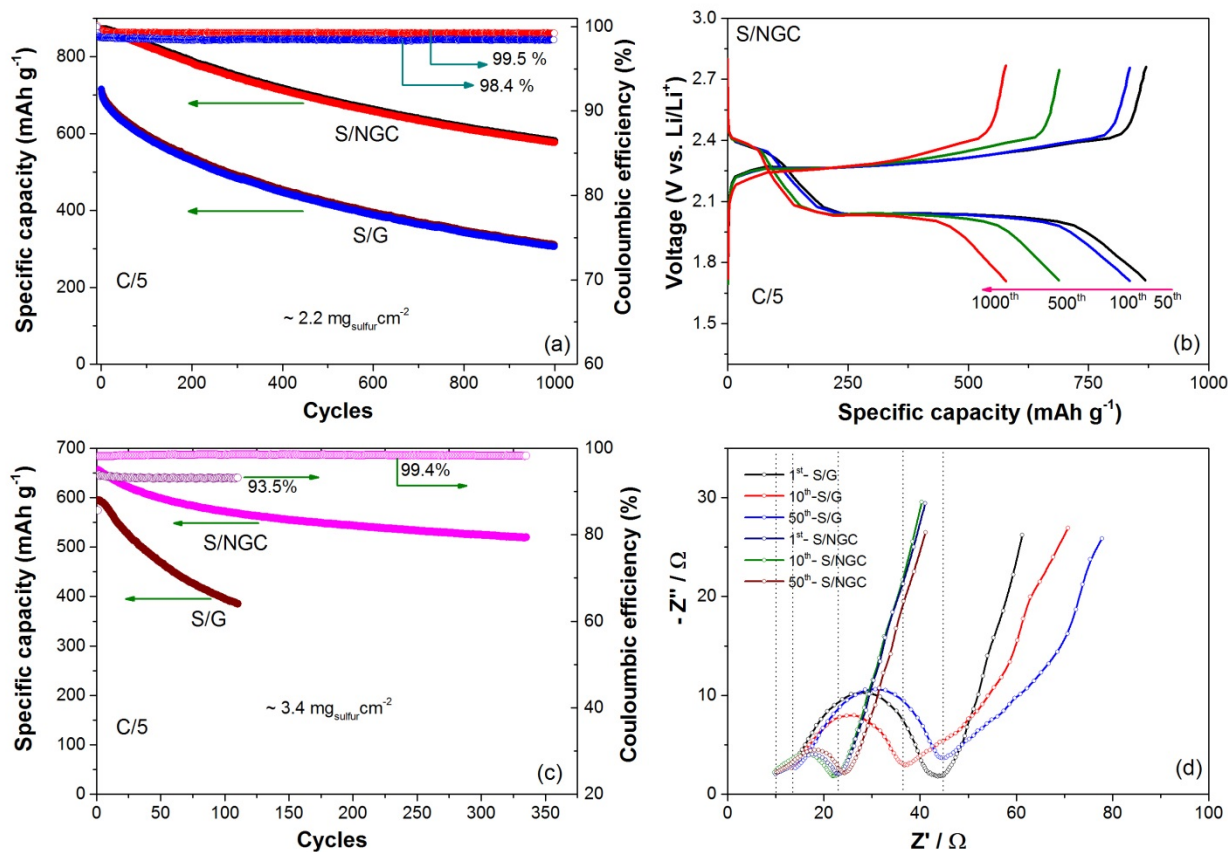


Figure 6. (a) Cycling performance of S/NGC and S/G electrodes with sulfur loading $\sim 2.2 \text{ mg}_{\text{sulfur}} \text{ cm}^{-2}$ for 1000 cycles at 0.2 C current rate, (b) galvanostatic discharge/charge voltage profiles of S/NGC at C/5 current rate for different cycles. (c) Cycling performance of S/NGC and S/G electrodes with a sulfur loading $\sim 3.4 \text{ mg}_{\text{sulfur}} \text{ cm}^{-2}$ for 1000 cycles at 0.2 C current rate, (d) ac impedance measurements of S/NGC and S/G electrodes at different cycles (1st, 10th, 100th cycles) after charge to 2.8 V.

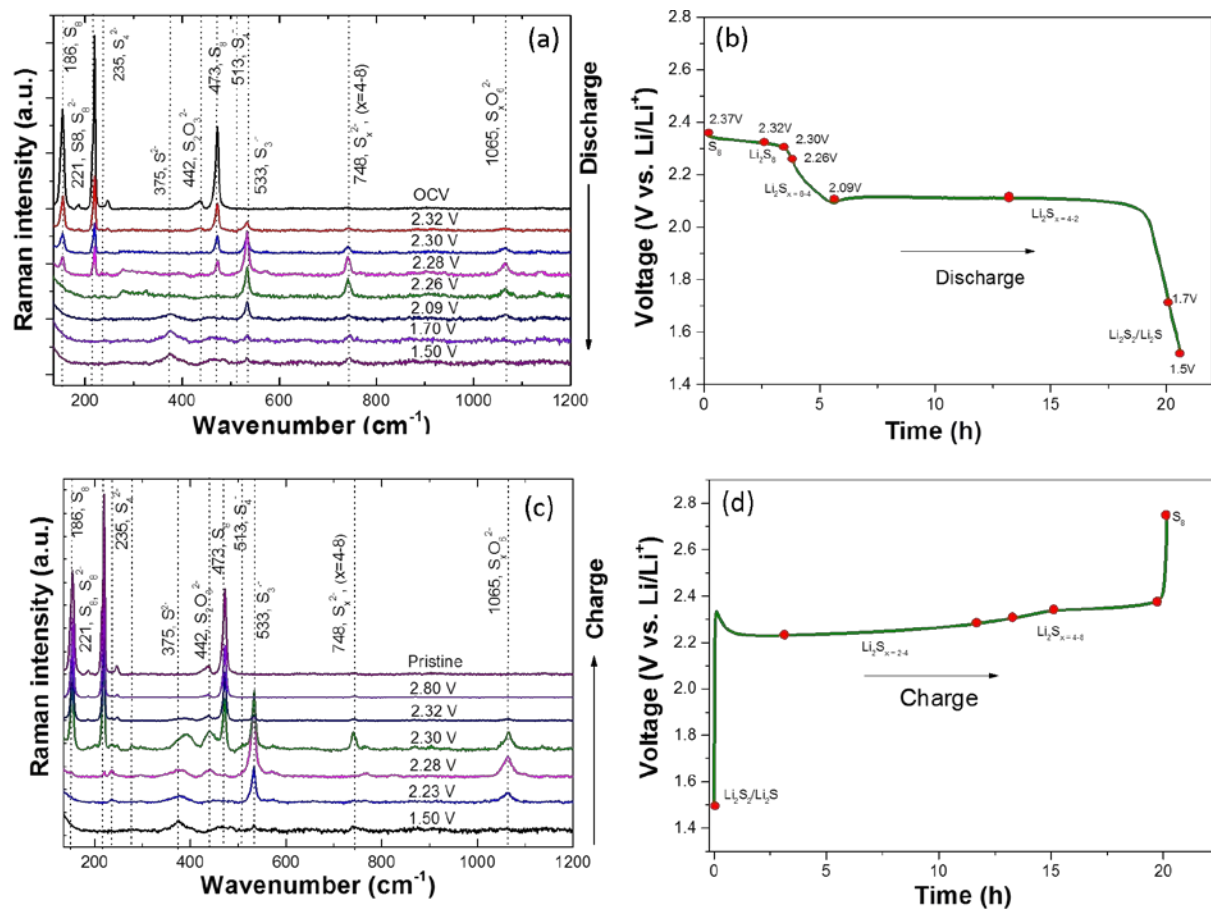


Figure 7. In-situ Raman spectra and associated voltage profiles obtained for S/NGC cathode during the discharge from 2.8 to 1.5 V (a, b), and during the charge from 1.5 to 2.8 V (c, d).

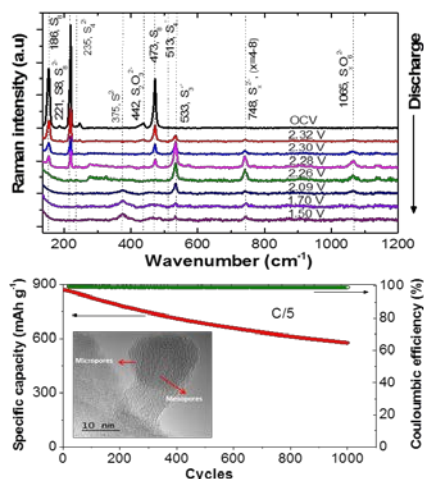
The table of contents

The superior performance of a newly designed, highly sulfur loaded carbon matrix (S/NGC) for Li/S batteries is demonstrated along with operando spectroscopy. The S/NGC material features a hierarchically organized micro/meso porous carbon matrix containing nitrogen and oxygen functional groups. S/NGC cathodes ($2.2 - 3.4 \text{ mg}_{\text{sulfur}} \text{ cm}^{-2}$) show long cycling stability (0.03 % average capacity decay per cycle for 1000 cycles) and more than 99 % coulombic efficiency.

Keyword: hierarchical porous materials, heteroatom doping, lithium-sulfur batteries, polysulfide dissolutions, in-situ Raman

Thomas Diemant, Xiu-Mei Lin, Musa Ali Cambaz, Ute Kaiser, R. Jürgen Behm, Maximilian Fichtner, Bhaghavathi Parambath Vinayan*

Nitrogen rich hierarchically organized porous carbon/sulfur composite cathode electrode for high performance Li/S battery: A mechanistic investigation by operando spectroscopic studies



ToC figure

Supporting Information

Nitrogen rich hierarchically organized porous carbon/sulfur composite cathode electrode for high performance Li/S battery: A mechanistic investigation by operando spectroscopic studies

*Bhaghavathi Parambath Vinayan**, *Thomas Diemant*, *Xiu-Mei Lin*, *Musa Ali Cambaz*, *Ute Kaiser*, *R. Jürgen Behm*, *Maximilian Fichtner*

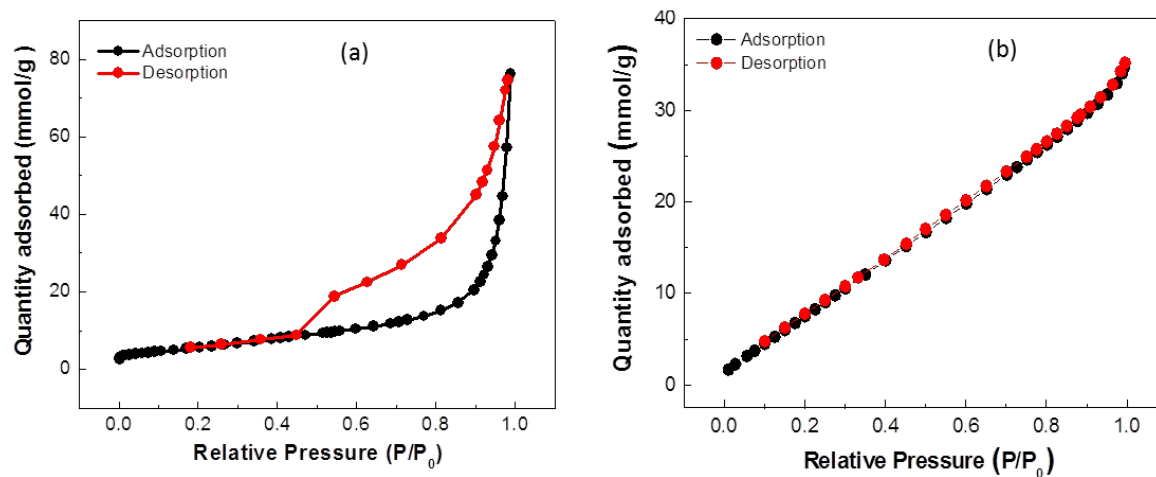


Figure S1: Nitrogen adsorption–desorption isotherms of graphene and nitrogen doped carbon matrix (NGC)

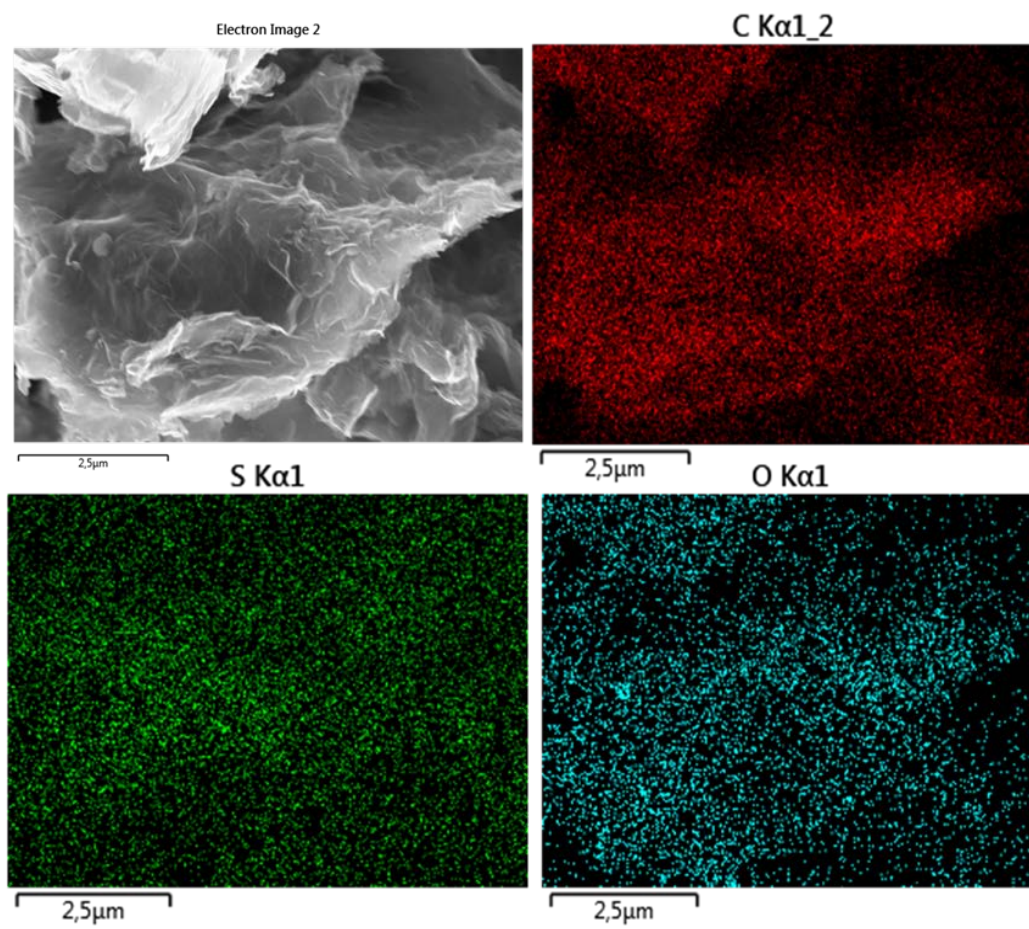


Figure S2: SEM and elemental mapping of S/G nanocomposite illustrating the uniform distribution of carbon, sulfur and oxygen.

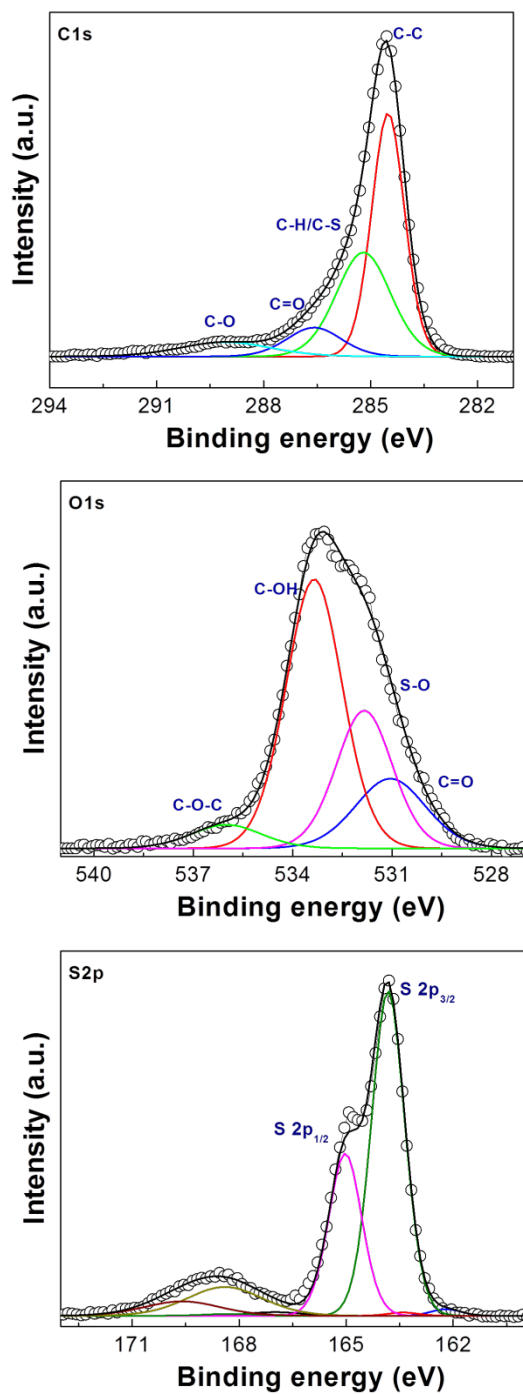


Figure S3: High resolution (a) C1s, (b) O1s and (c) S2p XP spectra of as prepared S/G nanocomposite.

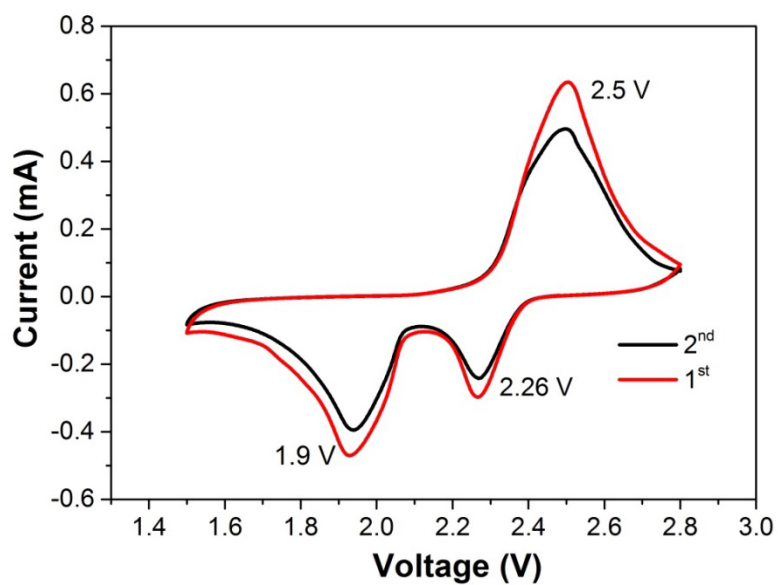


Figure S4: CV curve of S/G nanocomposite at 0.1 mV s^{-1} scanning rate.

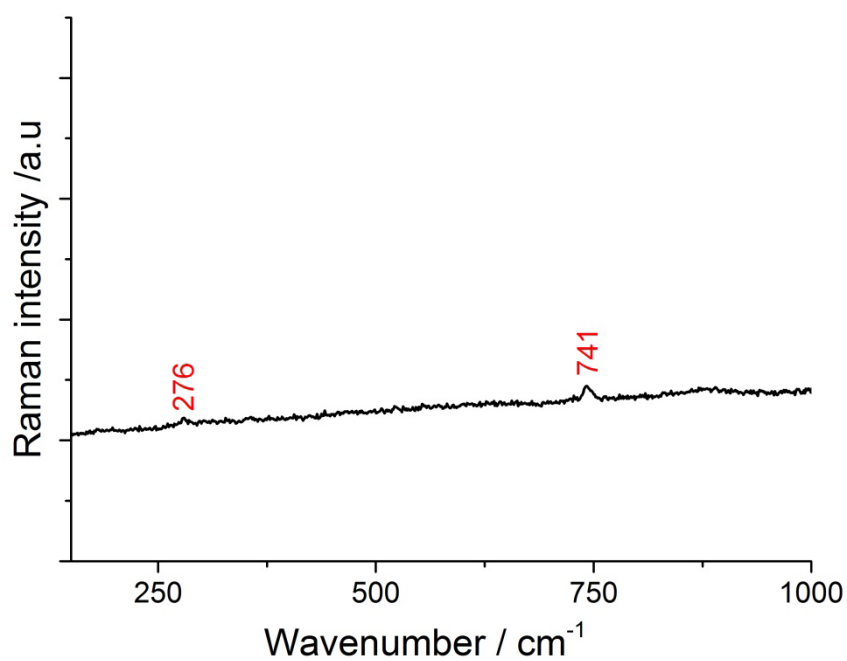


Figure S5: Raman spectra of 1 M LiTFSI electrolyte dissolved in a mixture of 1,3-dioxolane, dimethoxyethane and Pyr14TFSI (1:1:2 in volume) solvents.

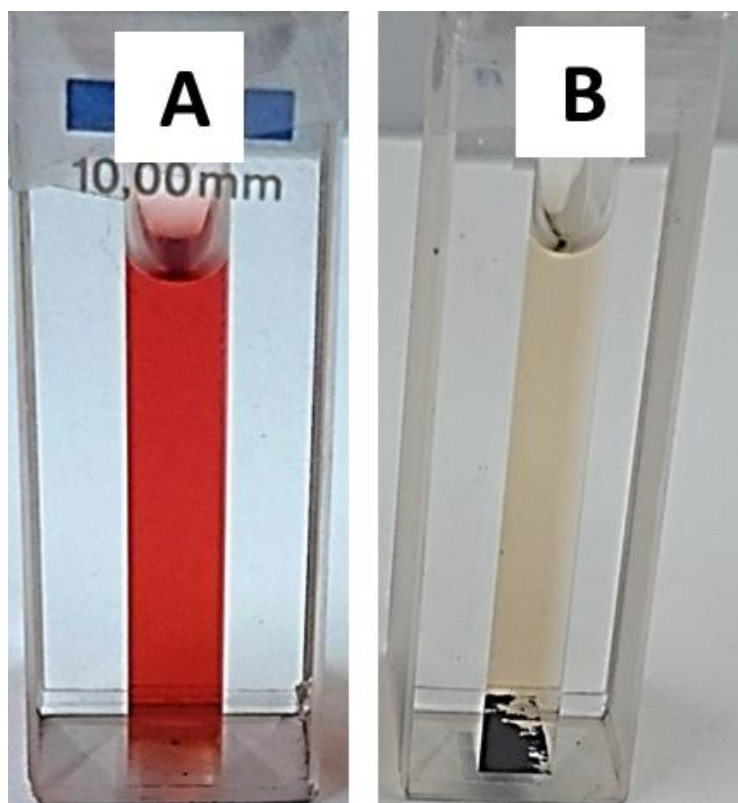


Figure S6: (A) Lithium polysulphides (Li_2S_8) solution and (B) Lithium polysulphides (Li_2S_8) solution after treating with NGC carbon matrix for two days.

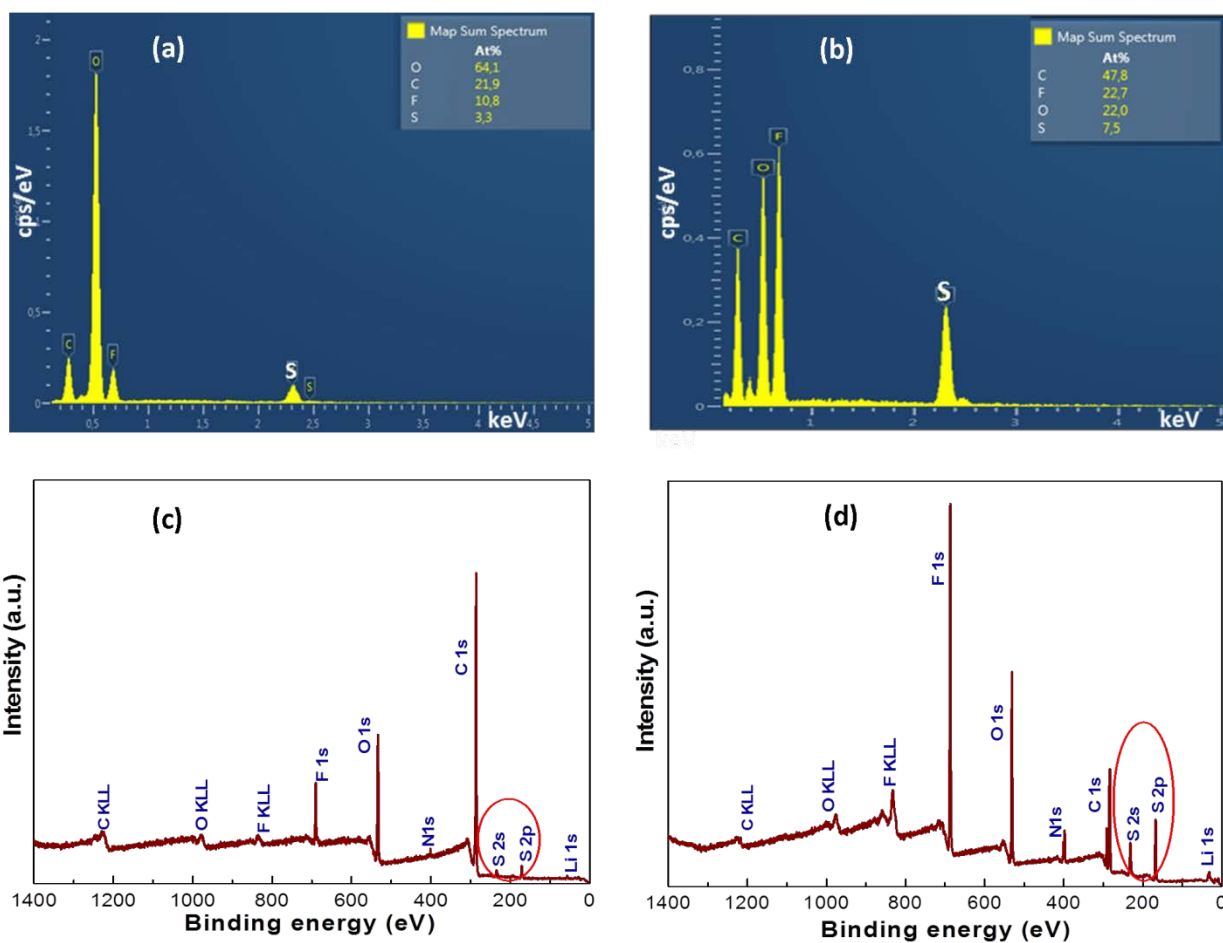


Figure S7: XPS and EDX measurements at the Li anode side of the cell with S/NGC (a, c) and S/G cathode electrodes (b, d).